Supporting information

for

Role of Catalyst Transformations, Defect Reconstruction, and Seawater Splitting under a Broad Solar Spectrum using MOF-derived (Cu)TiO_2 Model System

Bhavya Jaksani,[a,b] Hafijul Islam,[a,b] Harshini V Annadata,[c] Biplab Ghosh,[c] B. Moses Abraham,[d,e] Kathi Sudarshan,[f] Sanjoy Kr. Mahatha,[g] Ujjwal Pal,[a,b*] Indranil Mondal[h*]

[a]*Department of Energy & Environmental Engineering, CSIR-Indian Institute of Chemical Technology, Hyderabad, Telangana 500007, India.*

[b]*Academy of Scientific and Innovative Research (AcSIR), Ghaziabad 201002, India. Email: upal03@gmail.com; ujjwalpal@iict.res.in*

[c]*Beamline Development & Application Section, Bhabha Atomic Research Center, Mumbai 400085, India.*

[d]*A.J. Drexel Nanomaterials Institute, and Department of Materials Science and Engineering Drexel University, Philadelphia 19104, USA.*

[e]*Department of Chemical Engineering, Indian Institute of Technology Kanpur, Kanpur-208016, India.*

[f]*Radiochemistry Division, Bhabha Atomic Research Centre, Mumbai 400085, India*

[g]*UGC-DAE Consortium for Scientific Research, Khandwa Road, Indore, Madhya Pradesh 452001, India*

[h]*School of Chemistry, Indian Institute of Science Education and Research Thiruvananthapuram (IISER-TVM) Thiruvananthapuram, 695551, Kerala, India. Email: indraiict@gmail.com*

Corresponding author email: upal03@gmail.com (UP), indraiict@gmail.com (IM)

1. Experimental Section

1.1 Chemicals

Copper (II) nitrate trihydrate (Cu $(NO_3)_2.3H_2O$) ≥ 99%, trimesic acid (H_3BTC) 95%, N, N dimethyl formamide (DMF), Methanol (CH_3OH), commercial TiO_2 (P25) were obtained from the Sigma Aldrich. Titanium isopropoxide (Ti $\{OCH(CH_3)_2\}_4$) 97%, obtained from Avra. Ethanol (C_2H_5OH), Sodium chloride (NaCl), Potassium chloride (KCl), Magnesium chloride ($MgCl_2$) and Calcium chloride ($CaCl_2$). Commercial liquid humic acid (HuminOS, Casa De Amor, India) contains 10–12% humic acid (from natural leonardite), 3–5% fulvic acid, 3–6% K_2O, 10–12% organic carbon, and 0.5–1% chelated micronutrients (Fe, Zn, Mn), with water and stabilizers as balance components. In all the experiments distilled water (DI H_2O) was used. All the chemicals are commercially available and used without further purification.

1.2 Synthesis of photocatalysts

Synthesis of Cu-MOF(CuBTC): Firstly, dissolve 1.039 grams of copper nitrate ($Cu(NO_3)_2.3H_2O$) in 7.5 mL of deionized water. Next, in another round-bottomed flask, dissolve 0.903 grams of H_3BTC in a mixture of solution containing 7.5 mL of DMF and C_2H_5OH. The two solutions are combined and stirred for 30 minutes before transferring the mixture into a 100 mL Teflon-lined stainless-steel autoclave and solvothermal heated at 120°C for 12 h. After cooling the autoclave to room temperature, a blue precipitate is collected by centrifugation and washed three times with DMF followed by methanol and dried at 80 °C to yield the CuBTC. The Cu-MOF was synthesized following a previously reported method, with minor modifications.[1]

Synthesis of M-$CuTiO_2$: M-$CuTiO_2$ is synthesized by dispersing 100 mg of CuBTC in 20 mL of a 4:1 ethanol-water mixture in a round-bottom flask, followed by sonication for 30 minutes to ensure complete dispersion of the CuBTC particles. Subsequently, 2.5 mL of titanium isopropoxide ($Ti[OCH(CH_3)_2]_4$) was added dropwise under continuous stirring, which was maintained for 12 hours. The resulting precipitate was collected via centrifugation, washed three times with ethanol and water, and dried overnight in an oven. The final product was obtained by calcining the dried material at 450 °C for 5 h under N_2 atmosphere at a heating rate of 5 °C/min. The same procedure was repeated with a constant amount of titanium isopropoxide and varying amounts of CuBTC (10 mg, 50 mg, and 200 mg) to produce different levels of Cu-doped M-$CuTiO_2$. TiO_2 was synthesized using the same process, without adding the CuBTC.

Synthesis of Cu loaded TiO_2: Dissolve 240 mg of Cu $(NO_3)_2$. $3H_2O$ in a 100 ml D.I H_2O, and add 1g of TiO_2 into the same solution and sonicate the solution for 30 min. Next add $NaBH_4$ aqueous solution (Cu: $NaBH_4$ 1: 2.5) to the suspension and stir vigoursly for 24 h at room temperature. The product is collected by centrifugation, washed with water and dried at 80°C for overnight.[2]

Synthesis of E-Cu(0)TiO_2: Cu nanoparticles (Cu(0)) were synthesized via chemical reduction of 50 mg of $Cu(NO_3)_2 \cdot 3H_2O$ using freshly prepared $NaBH_4$ under vigorous stirring. The formation of Cu(0) was confirmed by the color change of the solution from blue to reddish-brown. After 1 h, the product was centrifuged and washed with water and ethanol. For E-Cu(0)/TiO_2 preparation, 5 mg of Cu nanoparticles was added to 100 mg TiO_2 dispersed in 20 mL ethanol and stirred overnight under N_2. The composite was centrifuged, washed with ethanol, dried at 60 °C, and used for photocatalytic studies.[3]

1.3 Preparation of photocatalyst film

The glass plate of dimension (1 cm x 3.5 cm) is thoroughly cleaned using acetone and soap water, and dried for an hour. The necessary quantities of photocatalyst (1 mg, 2 mg, 3 mg, and 5 mg) were added into 1 ml of ethanol and subjected to sonication for 30 minutes to achieve a uniform dispersion of the catalyst. The solution was uniformly drop casted on the glass plate with the help of micro-pipette and dried under room temperature. [4]

1.4 Preparation of simulated seawater

Dissolve 3.5 grams of sodium chloride (NaCl) in 100 mL of deionized (DI) water. [5]

1.5 Photocatalytic seawater splitting

Photocatalytic activity through the thin glass plate coated with the catalyst

The photocatalytic experiments for hydrogen production from seawater were conducted under simulated solar light using a 420 W xenon (Xe) lamp and 25 mL pyrex photoreactor. Glass plate coated with different amounts of M-CuTiO_2 (1mg, 2mg, 3mg and 5 mg) was introduced to the reactor containing 2 ml of methanol and 8 ml of simulated seawater. Then it was sealed with a rubber septum and a vacuum pump was used to remove oxygen from the system for 15 min and purging with Nitrogen for 15 min to eliminate dissolved air, then it was irradiated by a 420 W Xe lamp. Gas evolution was quantified by extracting gas samples from the reactor using a 100 µL airtight gas syringe, and subsequent analysis was performed using gas

chromatography equipped with a thermal conductivity detector (TCD) with N_2 as a carrier gas.

Photocatalytic activity through the catalyst dispersion

The photocatalytic experiments for hydrogen production from seawater were conducted under simulated solar light using a 420 W xenon (Xe) lamp and a 30 mL quartz photoreactor. A certain amount of M-$CuTiO_2$ was dispersed in 10 mL of an aqueous solution containing 2 mL of methanol and 8 mL of simulated seawater. The mixture solution was sealed in a quartz container, and a vacuum pump was used to remove oxygen from the system for 15 min and 15 min purging with Nitrogen to eliminate dissolved air, then it was stirred and irradiated by a 420 W Xe lamp. Gas evolution was quantified by extracting gas samples from the reactor using a 100 μL airtight gas syringe, and subsequent analysis was performed using gas chromatography equipped with a thermal conductivity detector (TCD) with N_2 as a carrier gas.

2. Characterization

The photocatalysts structural phase were analysed by Powder X-ray diffraction patterns (XRD) on a Bruker AXS diffractometer (D8 advance). The apparatus was operated at a 40 kV generator voltage and 30 mA current, with Cu-Kα1 irradiation applied (λ = 1.5406 Å). The sample was scanned at a rate of 1 s/step throughout the 2θ = 5-80° range. FTIR spectroscopy was used to characterize the surface features of the particles. The spectra were acquired using a Perkin Elmer FTIR spectrometer. X-ray photoelectron spectroscopy (XPS) was conducted using a Kratos Axis 165 analytical instrument with Mg Kα irradiation about 10^{-9} Torr pressure was maintained in the spectrometer. The structural morphology of the photocatalysts was analysed using MIRA3 FEG-SEM (TESCAN) scanning electron microscopy (SEM) at an accelerating voltage of 5 kV. Transmission electron microscopy (TEM) image of the representative photocatalysts was acquired using a JEOL 2010EX TEM apparatus, with a high-resolution objective-lens pole piece, at an acceleration voltage of 200 kV, and equipped with a CCD camera. The surface area of photocatalysts were determined by N_2 adsorption-desorption isotherms obtained from Quanta chrome Nova 2200e gas adsorption analyser at 77 K. The optical properties were characterized using UV-Vis diffuse reflectance spectroscopy (DRS) with a Perkin Elmer Lambda 750 instrument, employing $BaSO_4$ as a reference material. The sample has been positioned in the holder for measurement, allowing light to pass through it. This results in the absorption of light, and the transmitted light has been documented accordingly. The Photoluminescence (PL) spectra were obtained utilizing a Fluorolog-3

spectrofluorometer (Spex model, JobinYvon) at the corresponding excitation (λex) wavelength. Fluorescence Lifetime decay measurements were conducted utilizing a time-correlated single photon counting (TCSPC) setup (Fluorolog-3 Triple Illuminator, IBH Horiba Jobin Yvon). The samples were excited at 390 nm, with emission observed at approximately 480 nm. The Electron Paramagnetic Resonance (EPR) analysis was performed using a Bruker Model EMP-10/12/S spectrometer.

2.1 Positron annihilation lifetime spectroscopy (PALS)

Positron annihilation lifetime measurements were measured under ambient conditions on powder samples. Na-22 of 15 μCi deposited between two 8-micron polyimde films was used as positron source. The lifetime spectrometer is constructed from two BaF_2 scintillation detectors whose signals were digitized using DDRS4PALS software.[6] The time resolution of the spectrometer was 221 ps. The positron lifetime spectra were analysed using PALSfit3 software.[7]

2.2 Quasi In-situ UV-DRS and EPR

Real time Quasi in situ UV–DRS measurements were carried out using a PerkinElmer Lambda 750 spectrophotometer with $BaSO_4$ as the reflectance standard to monitor electronic and structural changes in the catalyst during photocatalysis. In a typical procedure, 50 mg of catalyst was dispersed in 50 mL of a water–methanol mixture in a quartz reactor, degassed for 10 min, and irradiated with a Xe lamp. At designated time intervals, 5 mL aliquots were withdrawn, centrifuged, and the recovered solids were subjected to UV–DRS analysis. The spectra obtained at each interval were compared with those of the catalyst before and after photocatalysis to evaluate the evolution of its optical properties.

Real time Quasi EPR measurements were carried out using a Bruker spectrometer equipped with a Bruker EMP-10/12/S system. The experimental conditions were: microwave frequency = 9.64 GHz, microwave power = 1 mW, modulation amplitude = 8 G, modulation frequency = 100 kHz, and gain = 50 dB. These measurements were performed to monitor the evolution of copper oxidation states during photocatalysis. After 2 h of irradiation, an aliquot of the reaction mixture was withdrawn, transferred into a nitrogen-purged quartz tube, and immediately subjected to EPR analysis. The obtained spectra were compared with those of the fresh and spent catalysts to assess the changes occurring under photocatalytic conditions.

2.3 X-ray absorption spectroscopy (XAS)

Room temperature X-ray Absorption Spectroscopy (XAS) measurements, including X-ray Near Edge Structure (XANES) and Extended X-ray Absorption Fine Structure (EXAFS) techniques at the Cu and Ti K-edges, were conducted at the Scanning EXAFS Beamline (BL-9) of the Indus-2 Synchrotron Source (2.5 GeV) at the Raja Ramana Centre for Advanced Technology (RRCAT), Indore, India. The beamline provided an energy resolution ($\Delta E/E$) of approximately 10^{-4} at 10 keV, utilizing a Si (111) double-crystal monochromator (DCM) with one flat crystal and another with bending capability for horizontal focusing. Vertical focusing was achieved through Rh/Pt-coated cylindrical grazing incidence mirrors, while a separate mirror was used for collimating the beam on the first crystal. Higher-order harmonics were effectively reduced by detuning the DCM.[8]

Reference spectra for Cu $(NO_3)_2$, commercial TiO_2, Cu_2O were recorded at ambient conditions using 10 mm pellets. These pellets were prepared by binding powdered samples with cellulose and analysed in transmission mode. Measurements employed two ionization chambers, each 30 cm in length, to record the incident (I_0) and transmitted (I_t) X-ray fluxes. The absorption coefficient (μ) was determined using the relation $\mu x = -\ln (I_t/I_0)$, where x denotes the thickness of the sample along the path of the X-ray beam.

The Cu and Ti K-edge spectra for TiO_2 and M-$CuTiO_2$ (before and after reaction) samples were collected in fluorescence mode. A silicon drift detector was used to measure the fluorescence signal (I_f), while the ionization chamber captured the incident X-ray flux (I_0). The absorption coefficient in fluorescence mode was calculated as $\mu = I_f/I_0$.

Data Analysis of XAS

Data reduction and fitting were performed using the Demeter software suite, equipped with Strawberry Perl (version 0.9.25).[9] The analysis involved isolating the oscillatory component of the EXAFS signal from the absorption spectrum $\mu(E)$ by removing the background contribution from the sample's atomic absorption. This signal was subsequently converted to a wave number-dependent absorption coefficient. Finally, a Fourier transform was applied to generate $\chi(R)$ versus R plots, providing structural information about the local environment around the absorbing atom.

2.4 Photo-electrochemical studies

Photoelectrochemical measurements at room temperature were recorded on the CH Instruments Inc., USA, CHI6005E, Electrochemical Workstation with Potentiostat using a standard three-electrode system with the photocatalyst-coated ITO as the working electrode, Pt

wire as the counter electrode, SCE electrode as the reference electrode. The artificial solar simulator of AM 1G illuminator (100 mW cm^{-2}) was used as the light source during the measurement. The electrochemical cell was a conventional three electrode cell with a Pyrex glass. A 0.25 M Na_2SO_4 solution was used as the electrolyte. The preparation of the working electrode is carried out using 20 µL of suspension (5 mg in 1mL ethanol) on ITO coated glass surface with a geometric area of 4 cm^2. The Mott-Schottky plots were conducted at frequency of 1000 Hz to determine the flat-band potential and donor density. The donor densities of TiO_2 and M-$CuTiO_2$ from mott Schottky plots were calculated by using following equation

$$N_D = \frac{2}{\epsilon_r \, \epsilon_0 \, A^2 q \, m} \qquad (S1)$$

N_D= Donor density

ϵ_r = Relative permittivity of semiconductor (Here is assumed to be 50 F. cm^{-1}) [10]

ϵ_0 = Permittivity of free space (8.85 10^{-14} F. cm^{-1})

A = Area of electrode (4 cm^2)

q = Electronic charge (1.60 10^{-19} C)

m = Slope of mott Schottky plot.

2.5 Preparation of KI- Starch solution for chlorine detection

Dissolve 1 g of soluble starch powder in 100 mL of deionized (D.I.) water and heat the solution gently while stirring until the starch is fully dissolved, forming a clear solution. After cooling to room temperature, add 0.5 g of potassium iodide (KI) and mix thoroughly until a homogeneous solution is obtained. To test for chlorine, a few drops of the prepared KI-starch solution were added to the photocatalytic reaction mixture. The presence of chlorine would be indicated by a blue-black colour change due to the oxidation of iodide (I^-) to iodine (I_2), which forms a complex with starch. However, in our experiment, no colour change was observed upon addition of the KI-starch solution, confirming that chlorine was not formed during the reaction.

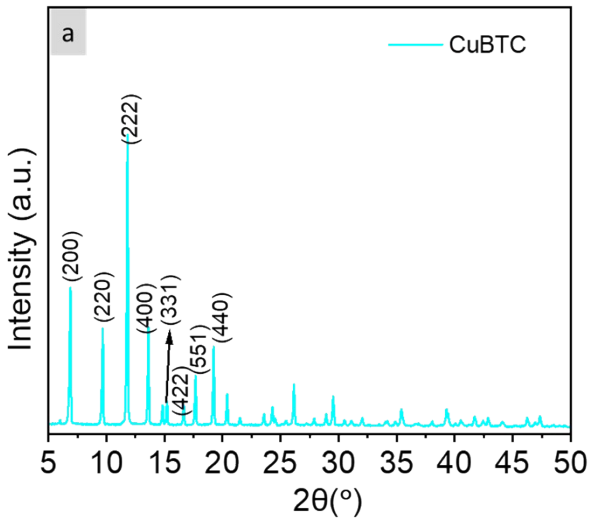

Fig. S1. (a)PXRD of Cu-BTC. The data were recorded with same experimental procedure as used in the previous report.[11]

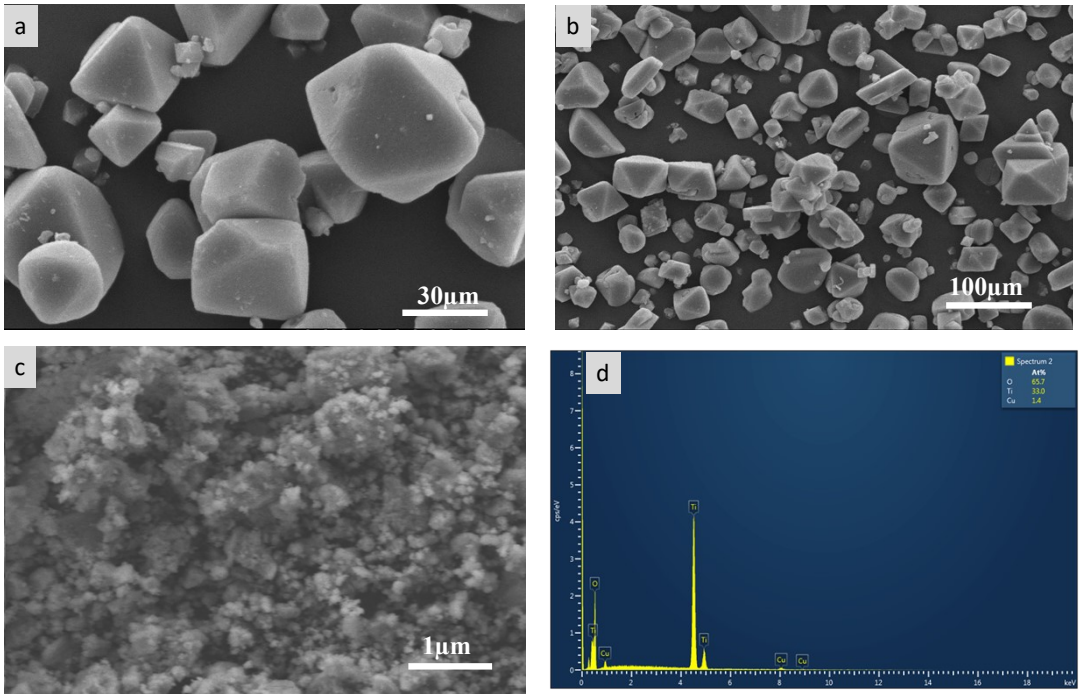

Fig. S2. FESEM images of (a, b) as-prepared Cu-BTC, and (c) M-$CuTiO_2$. (d) EDX profile of M-$CuTiO_2$. We detected a carbon content of around 4% after annealing in the M-$CuTiO_2$

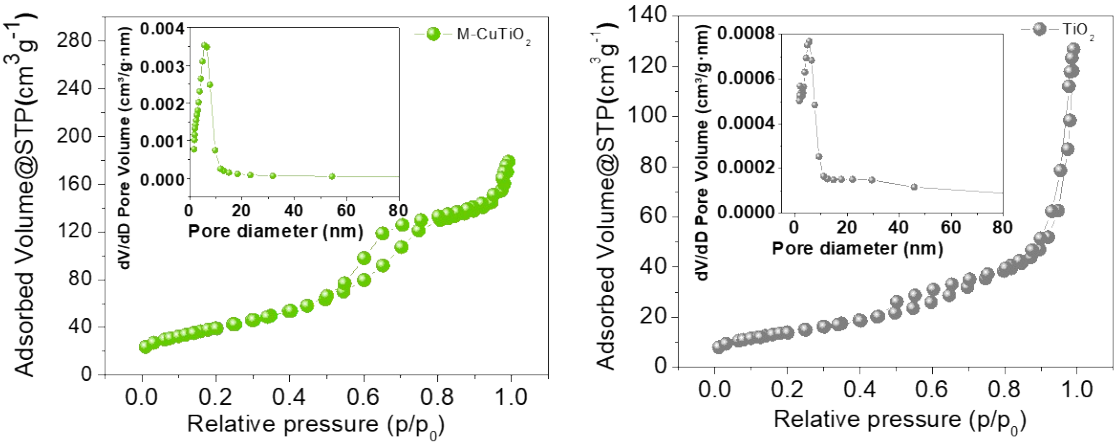

Fig. S3. BET isotherm graphs of (a) M-$CuTiO_2$ (b) TiO_2. (Inset Figures displaying the BJH pore size distribution curves).

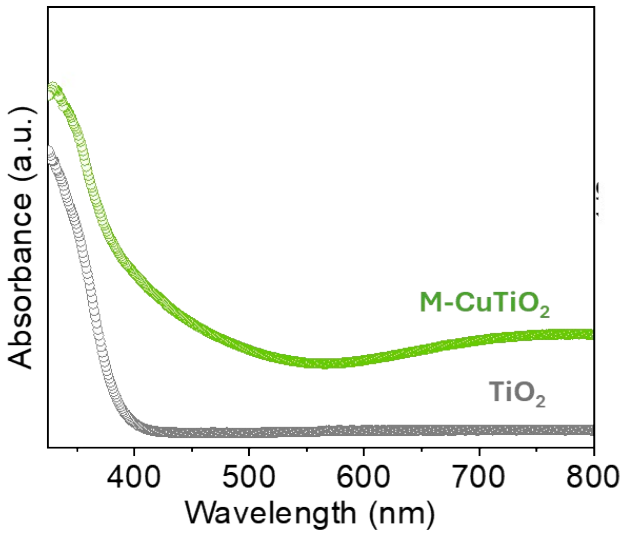

Fig. S4. Optical absorption spectra of as-prepared TiO_2 and M-$CuTiO_2$. The broad and weak absorption of M-$CuTiO_2$ is attributed to the typical *d-d* transition of Cu^{2+}. In this composite photoexcitation does not occur in the visible region.

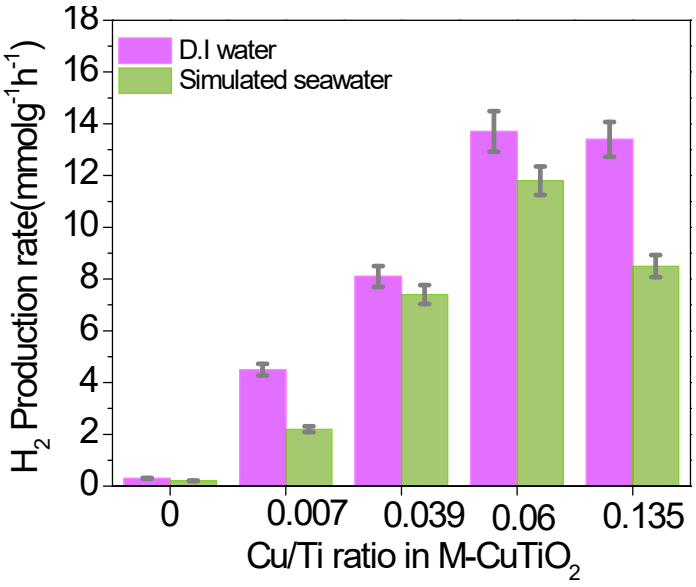

Fig. S5. Photocatalytic hydrogen production of synthesized photocatalyst in natural water and simulated seawater.

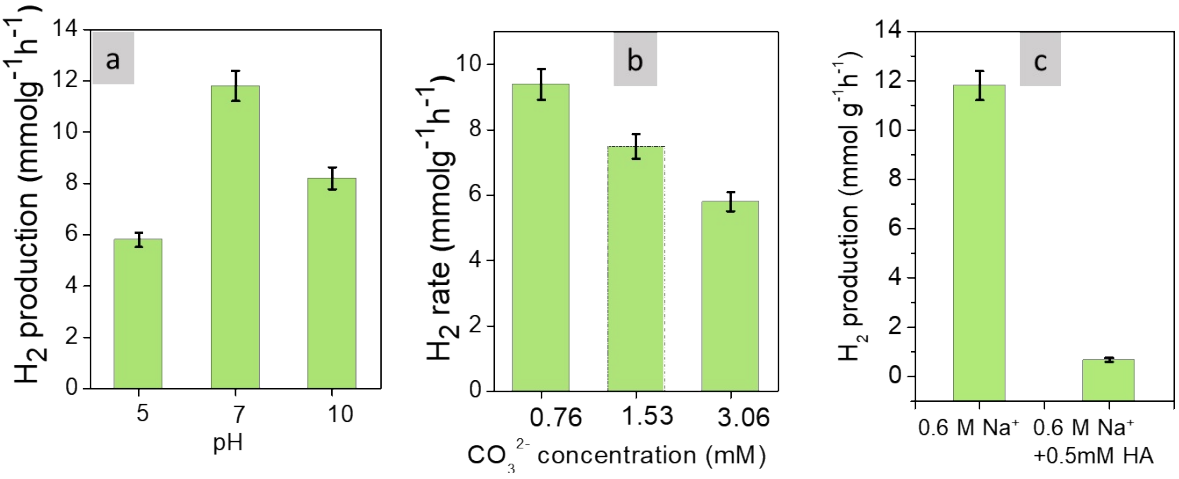

Fig. S6. Photocatalytic activity of the M-$CuTiO_2$ in different simulated seawater solutions containing 0.6 M NaCl and 20 vol% of methanol. (a) pH variation done using 0.1 M HCl and 0.1 M NaOH, (b) CO_3^{2-} concentration variation, and (c) effect of humic acid.

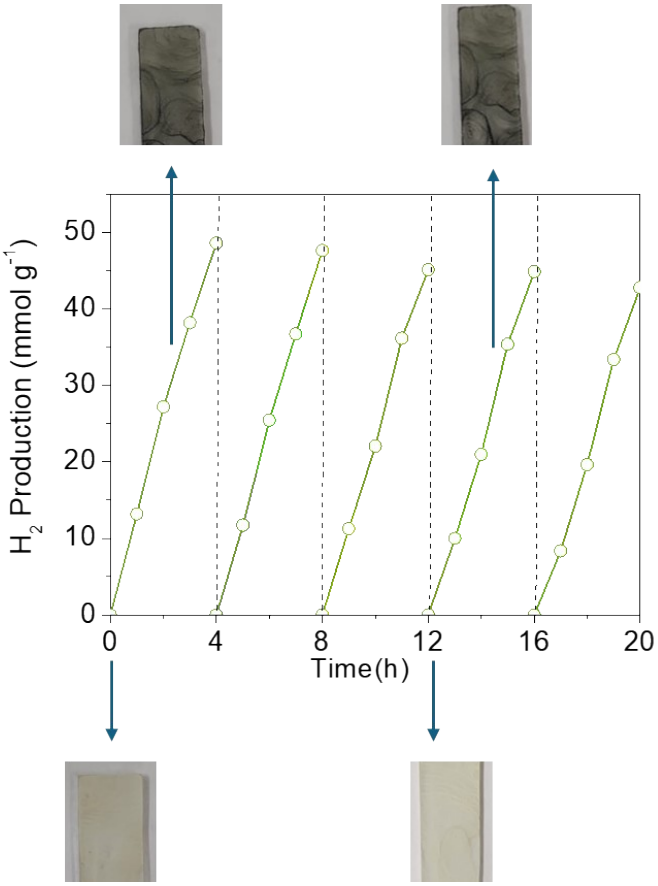

Fig. S7. Photocatalytic hydrogen production recyclability test of M-$CuTiO_2$ under simulated sunlight in the simulated seawater (using 0.6 M NaCl solution). The color of the catalyst film is also depicted at different course of the recyclability test. The bright colors appeared after the catalyst film is exposed to air for a significant time. The dark color appeared during the reaction and only sustained for a few minutes when exposed to ambient conditions. The change of this color is reproducible.

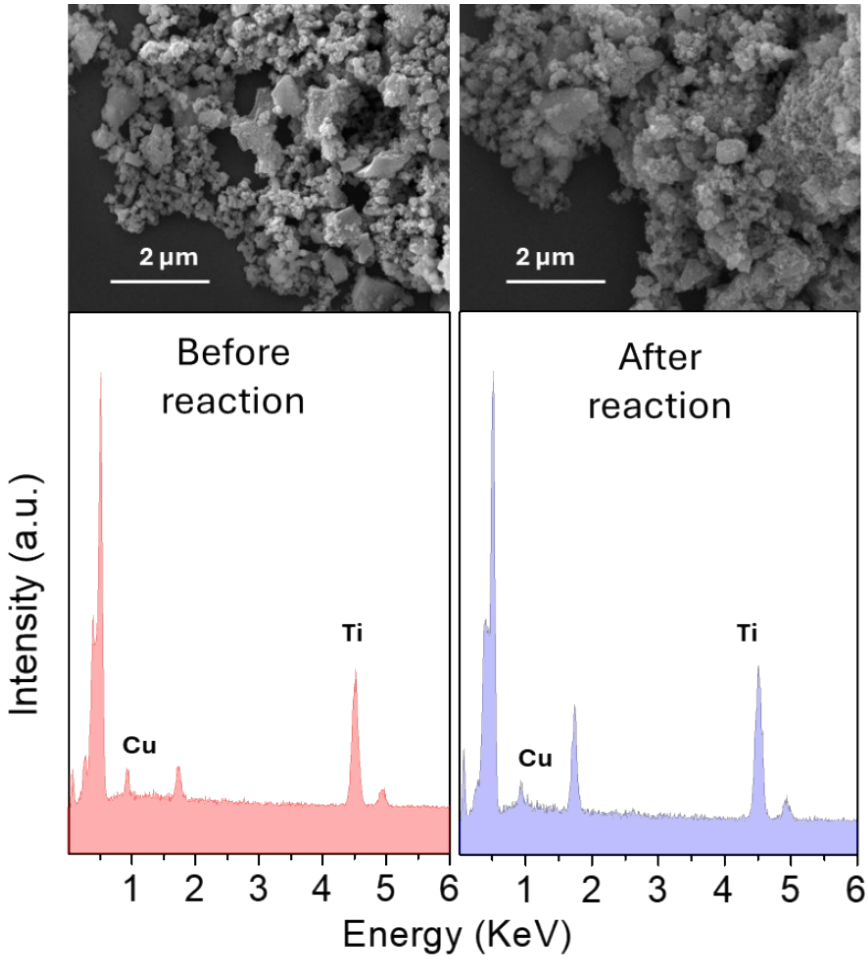

Fig. S8. SEM of the M-$CuTiO_2$ before and after the photocatalytic reactions (see Fig. 3d, main text). The SEM-EDX detected Cu/Ti ratio before and after reaction was 0.064 and 0.043.

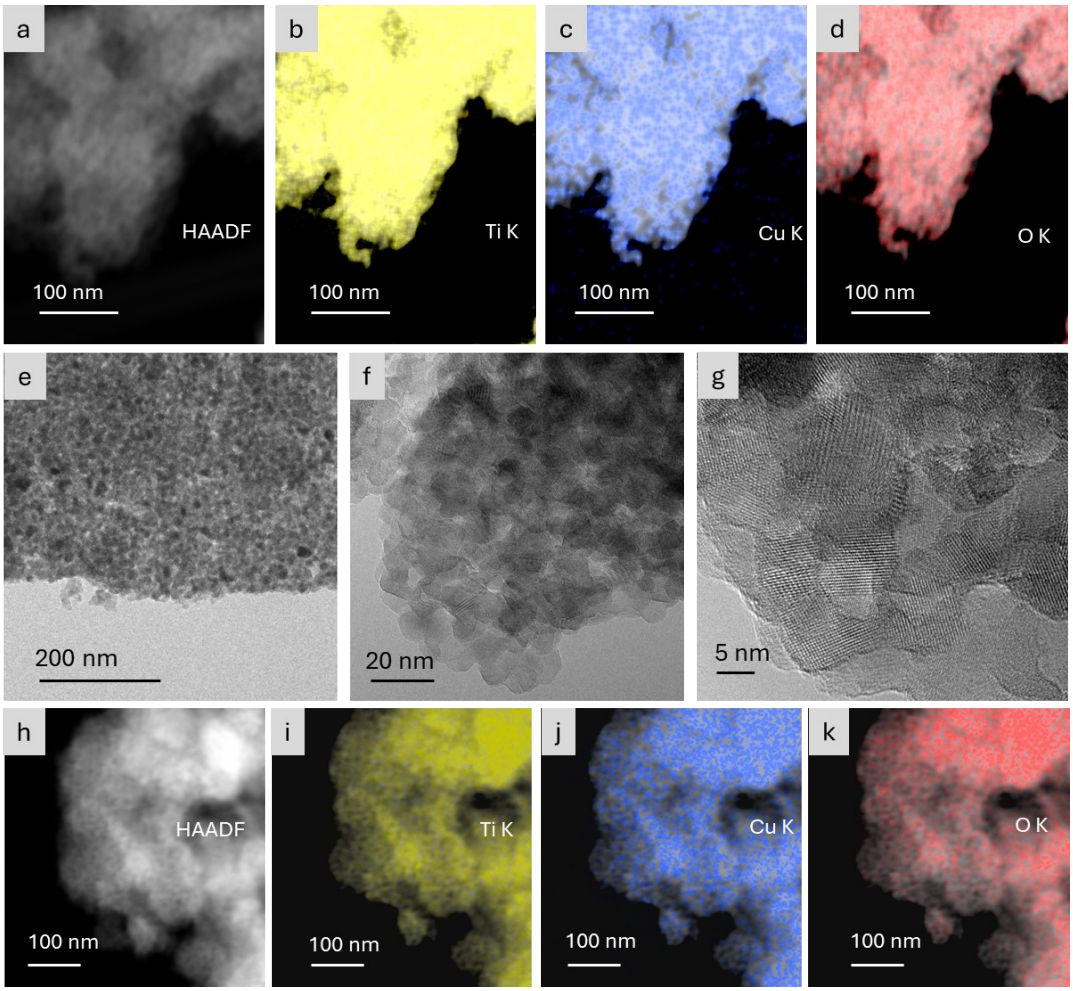

Fig. S9. (a) HAADF and (b-d) corresponding elemental mapping of the Ti, Cu, and O of the as-prepared M-$CuTiO_2$. (e, f) TEM and (g) HRTEM image of after reaction (see Fig. 3d) M-$CuTiO_2$ sample. In the HRTEM, we have seen similar defect-rich features for the CuO_x and TiO_2 interface as observed in the before reaction. (h) HAADF and (i-k) corresponding elemental mapping for the Ti, Cu, and O in the post-reaction sample. No phase segregation was detected within the nanostructures.

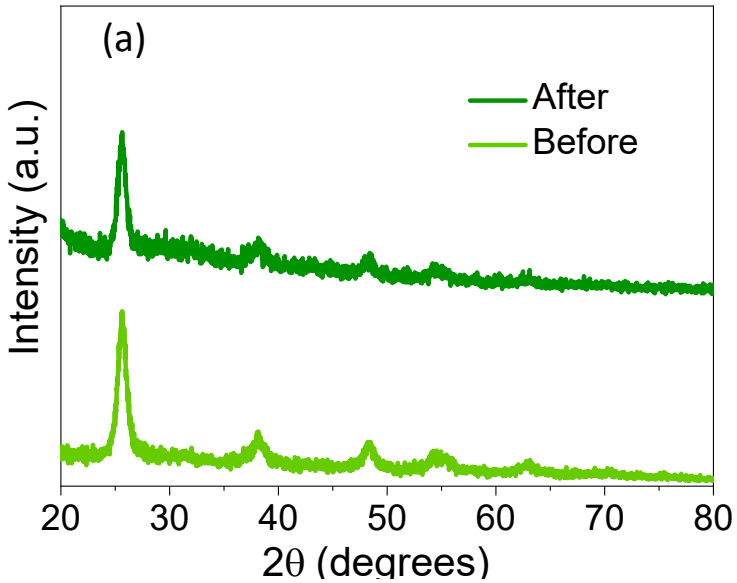

Fig. S10. PXRD of M-CuTiO$_2$ before and after photocatalytic reaction (see Fig. 3d main text).

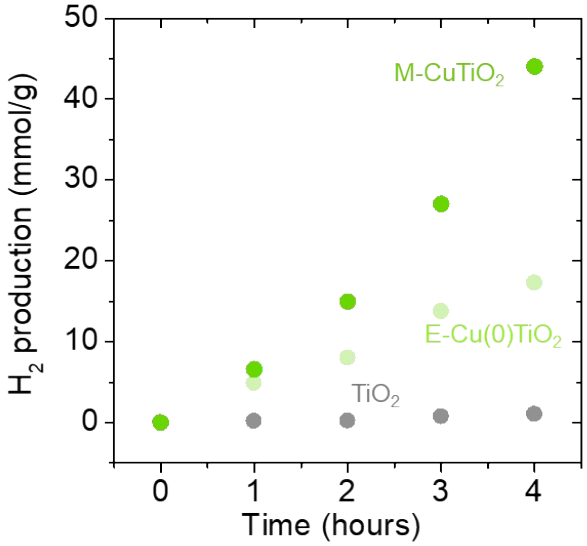

Fig. S11. Photocatalytic activity comparison among different Cu/TiO$_2$ catalysts. TiO$_2$ was prepared using the same procedure as M-CuTiO$_2$, except using MOF. For E-Cu(0)TiO$_2$, Cu(0) is externally synthesized using borohydride[3] and mixed with separately prepared TiO$_2$ (as mentioned before). For this experiment, the copper content in E-Cu(0)TiO$_2$ was kept similar.

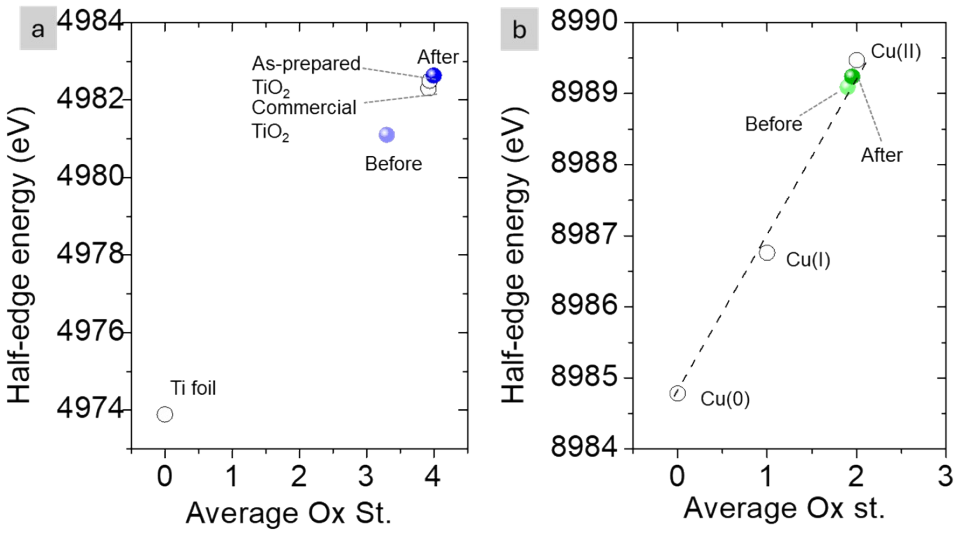

Fig. S12. Semiquantitative oxidation state estimation of (a) Ti from Ti-K and (b) Cu from Cu-K XANES half-edge energy measurements of the as-prepared M-CuTiO$_2$ before and after reaction, and compared with that of reference samples.

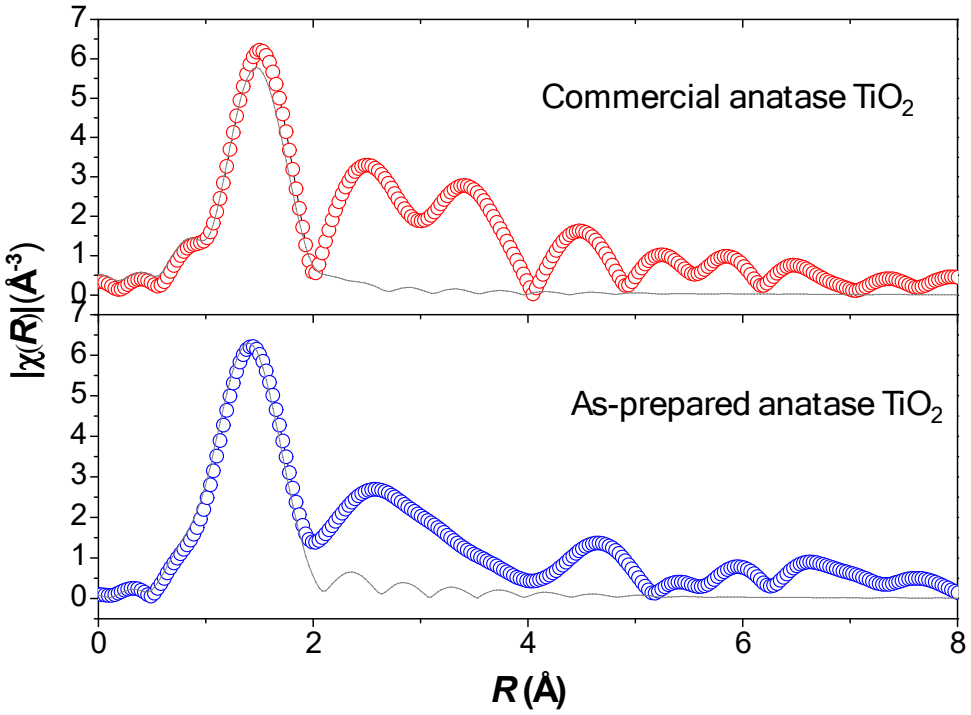

Fig. S13. T-K edge EXAFS spectra of the as-prepared TiO$_2$ and commercial TiO$_2$ with simulations in grey.

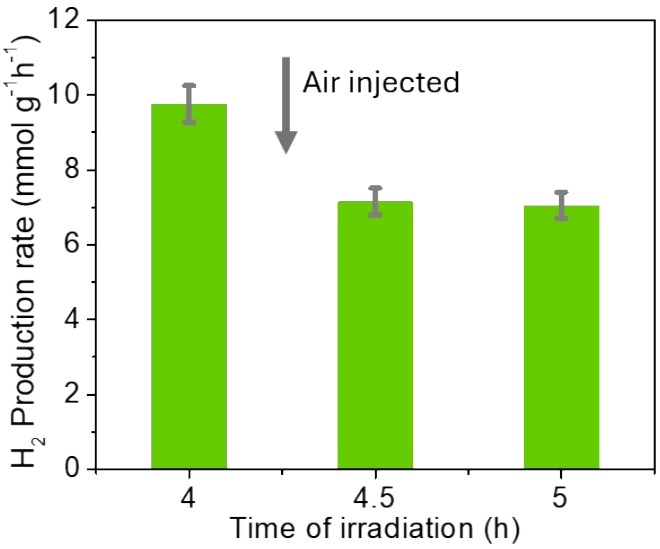

Fig. S14. Bar diagram showing the decrease in the H_2 activity after injecting 5 ml of air bubble through the catalyst dispersion inside the photoreactor.

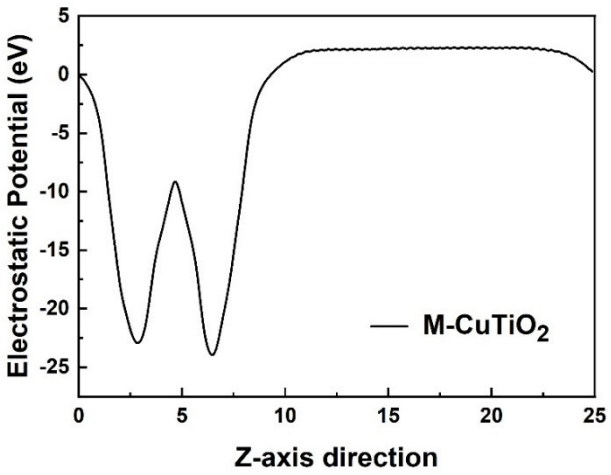

Fig. S15: Computed electrostatic potential of M-$CuTiO_2$

Table S1. Cu/Ti ratio of M-$CuTiO_2$ composite before and after (see Fig. 3d) photocatalytic reaction. The best catalytic results are obtained for the composite with a Cu/Ti ratio of ~0.06. Other composites were not detected after reactions.

Samples	**Cu/Ti ratio before reaction**	**Cu/Ti ratio after reaction**
M-$CuTiO_2$ (100 mg Cu-BTC used). This sample was used for the detailed catalytic analysis	0.064 (SEM-EDX) 0.06 (ICP)	0.043 (SEM-EDX) 0.04 (ICP)
M-$CuTiO_2$ (10 mg Cu-BTC used)	0.007 (ICP)	-
M-$CuTiO_2$ (50 mg Cu-BTC used)	0.039 (ICP)	-
M-$CuTiO_2$ (200 mg Cu-BTC used)	0.135 (ICP)	-

Table S2. Surface area and pore size parameters of the as-prepared catalysts.

S. No	**Photocatalyst**	**BET surface area (m^2g^{-1})**	**Pore size (Å)**	**Pore volume (cm^3g^{-1})**
1	TiO_2	51.69	7.62	0.69
2	M-$CuTiO_2$	145.66	6.19	0.22

Table S3. Positron annihilation lifetimes and intensities

Sample ID	**τ_1 (ps)**	**I_1 (%)**	**τ_2 (ps)**	**I_2 (%)**	**τ_{avg} (ps)**	**τ_3 (ns)**	**I_3 (%)**
Cu loaded TiO_2	281 ± 7	61 ± 6	422 ± 14	39 ± 6	336 ± 32	2.0 ± 0.1	0.5 ± 0.1
M-$CuTiO_2$	296 ± 4	84 ± 5	444 ± 30	15 ± 5	319 ± 26	1.6 ± 0.1	0.5 ± 0.1

Table S4. Photocatalytic hydrogen evolution from various sources of water through the final catalyst.

S. No.	Reaction medium	H_2 production ($mmolg^{-1}h^{-1}$)
1	Natural seawater	3.9
2	D. I water	13.7
3	Simulated seawater	11.8

Table S5. Photocatalytic hydrogen evolution from various concentration of NaCl solution through final catalyst

S. No.	Concentration of NaCl solution (mM)	H_2 production ($mmolg^{-1}h^{-1}$)
1	0	13.7
2	300	12.8
3	600	11.8
4	1200	4.8

Table S6. Photocatalytic hydrogen evolution from various metal aqueous salt solution through final catalyst.

S. No.	Reaction medium	H_2 production ($mmolg^{-1}\ h^{-1}$)
1	D.I Water	13.7
2	NaCl solution	11.8
3	KCl solution	2.6

4	$MgCl_2$ solution	1.4
5	$CaCl_2$ solution	0.9

Table S7. estimation of hydrogen production from CH_3OH sacrificial electron donor. Since the FID detector detects a trace amount of CH_3OH, we conduct the reaction with 5% CH_3OH in 10 ml of reaction mixture. It was observed that almost 28.5% hydrogen was coming from CH_3OH (simply if we assume all the CH_3OH is converting into CO_2 and H_2 using H_2O).

Timestamp	**Area of CH_3OH in GC FID**	**H_2 yield in 15 ml headspace using 2 mg of catalyst**
Before reaction	498753.53	-
After 4 h of reaction	157328.11	0.05 mmol

Table S8. Photocatalytic hydrogen evolution activity from D.I water and simulated seawater through thin films

S. No.	**Cu/Ti ratio in M-$CuTiO_2$**	**H_2 production ($mmolg^{-1}h^{-1}$)**	
		D. I water	**Simulated seawater**
1	0	0.3	0.2

2	0.007	4.5	2.2
3	0.039	8.1	7.4
4	0.06	13.7	11.8
5	0.135	12.4	8.5

Table S9. Photocatalytic hydrogen evolution activity of M-CuTiO$_2$ from simulated seawater through thin films through natural sunlight.

Day	**H_2 Production rate ($mmolg^{-1}h^{-1}$)**
1	2.1
2	4.4
3	6.2
4	5
5	5.5
6	4.9
7	6
8	4.6
9	4.3
10	2.7

Table S10. Comparative table of various photocatalysts for photocatalytic hydrogen evolution from seawater/simulated seawater.

S. no	Catalyst composition	Light source & sacrificial agent &cocatalyst	H_2 production (mmol g^{-1} h^{-1})	Reaction medium	REF
1	0.5wt%TiO_2/Cu_2O	300 W Xe lamp & Methanol & H_2PtCl_6	17.90	Natural Seawater	[12]
2	mesoporous brookite/anatase TiO_2	500 W Hg Lamp	6.49	Natural seawater	[13]
3	Co-RuO_x/TiO_2	300 W Xe lamp & TEOA	9.83	Natural seawater	[14]
4	TiO_2/RuO_2	300 W Xenon lamp & Methanol	14.89	Simulated seawater	[15]
5	TiO_2/1T-rich$MoSe_2$	300 W Xe lamp & methanol	1.89	Synthetic seawater	[16]
6	0.3wt% Pt/TiO_2	500 W Xe lamp &	1.57	Natural seawater	[17]

		Glycerol			
7	V_{ti}-TiO_2	PLS-SXE-300D lamp & methanol & H_2PtCl_6	25.90	Simulated seawater	[18]
8	WS_2/C-TiO_2/g-C_3N_4	300 W Xe lamp & TEOA	0.98	Natural seawater	[19]
9	N vacancies in g-C_3N_4/ZIF-8	500 W xenon lamp & methanol & H_2PtCl_6	0.11	Natural seawater	[20]
10	Cu_2O/TiO_2	300 W Xe lamp & Methanol	5.10	Natural seawater	[21]
11	Ti-O-Si	300 W Xe lamp & TEOA	1.60	Simulated seawater	[22]
12	V_N-HCN	300W Xe lamp & methanol & H_2PtCl_6	8.70	Natural seawater	[23]
13	H-CoS/CdS	visible light ($\lambda > 420$ nm) & Na_2S/Na_2S	0.57	Simulated seawater	[24]

		O_3			
14	CDs/CdS	300W Xe lamp & lactic acid	4.64	Natural seawater	[25]
15	CuO/nano TiO_2	300 W Xenon arc lamp	0.15	Natural seawater	[26]
16	Cu0.5/CdS-H	300 W Xe lamp ($\lambda \geq$ 420 nm) & lactic acid	17.8	Alkaline seawater	[27]
17	**M-CuTiO$_2$**	**420 W Xe lamp and Methanol**	**11.8**	**Simulated seawater**	**This work**
18	**M-CuTiO$_2$**	**420 W Xe lamp and Methanol**	**3.90**	**Natural seawater**	**This work**

Table S11. The best fits to the EXAFS data were performed in *R*-space for the first Ti-O coordination shell in both M-$CuTiO_2$ samples before and after reaction. The fitting results (*R*: Ti-O bond length in Å ; *N*: coordination number; σ^2: Debye-Waller factor and R-factor: goodness of fit) for the Ti K-edge are given in the below table.

Path	**Parameters**	**Commercial TiO_2**	**Prepared TiO_2**	**M-$CuTiO_2$ (Before reaction)**	**M-$CuTiO_2$ (After reaction)**
Ti-O	*R* (Å)	1.95 ± 0.03	1.90 ± 0.03	1.90 ± 0.02	1.96 ± 0.01
	N	6.1 ± 0.9	4.0 ± 0.7	1.9 ± 0.3	5.0 ± 1.0
	σ^2	0.008	0.008	0.001	0.001
	R-factor	0.013	0.020	0.014	0.016

Table S12. The best fits to the EXAFS data were performed in *R*-space for the first Cu-O coordination shell in both MOF samples before and after reaction. The fitting results (***R***: Cu-O bond length in Å ; ***N***: coordination number; $\boldsymbol{\sigma^2}$: Debye-Waller factor and **R-factor**: goodness of fit) for the Cu K-edge are given in the below table.

Path	**Parameters**	**M-$CuTiO_2$ (Before reaction)**	**M-$CuTiO_2$ (After reaction)**
Cu-O	*R* (Å)	1.86 ± 0.02	1.94 ± 0.02
	N	3.2 ± 0.4	2.7 ± 0.2
	σ^2	0.002	0.002

References

1. X. Xue, Y. Weng, S. Yang, S. Meng, Z. Zhang, G. Yi and Y. Zhang, *Environ. Sci. Pollut. Res.* **2021**, 28, 15883-15889.
2. Q. Shi, G. Ping, X. Wang, H. Xu, J. Li, J. Cui, H. Abroshan, H. Ding and G. Li, *J. Mater. Chem. A*, **2019**, 7, 2253-2260.
3. G. N. Glavee, K. J. Klabunde, C. M. Sorensen and G. C. Hadjipanayis, *Langmuir*, **1994**, 10, 4726-4730
4. N. Nalajala, K. K. Patra, P. A. Bharad and C. S. Gopinath, *RSC Adv* ., **2019**, 9, 6094-6100.
5. V.-H. Dang, T.-A. Nguyen, M.-V. Le, D. Q. Nguyen, Y. H. Wang, J. C. S. Wu, *Chem. Eng. J.* **2024**, 484, 149213.
6. D. Petschke and T. E. M. Staab, *SoftwareX*, **2019,** 10, 100261.
7. J. V. Olsen, P. Kirkegaard and M. Eldrup, *AIP Conf. Proc.*, **2019**, 2182.
8. A. K. Poswal, A. Agrawal, H. K. Poswal, D. Bhattacharyya, S. N. Jha, N. K. Sahoo, *J. Synchrotron Rad.,* **2016**, 23, 1518-1525.
9. B. Ravel, M. J. S. R. Newville, *J. Synchrotron Rad.* **2005**, 12, 537-541.
10. P. Pu, H. Cachet and E. M. M. Sutter, *Electrochimica Acta*, **2010,** 55, 5938-5946.
11. B. Jaksani, R. Chauhan, S. D. Kshirsagar, A. Rana, U. Pal and A. K. Singh, *Chem Comm*, **2024**, 60, 14212-14215.
12. S.-T. Xiao, S.-M. Wu, L. Wu, Y. Dong, J.-W. Liu, L.-Y. Wang, X.-Y. Chen, Y.-T. Wang, G. Tian, G.-G. Chang, M. Shalom, P. Fornasiero and X.-Y. Yang, *ACS Nano*, **2023**, 17, 18217-18226.
13. Z. Cheng, X. Zhang, C. Bo, Y. Sun, C. Li, L. Piao, *Int. J. Hydrog. Energy* **2024**, 55, 542-549.
14. J. Shen, C. Luo, S. Qiao, Y. Chen, K. Fu, J. Xu, J. Pei, Y. Tang, X. Zhang, H. Tang, *Adv. Funct. Mater.* **2024**, 2309056.
15. H. Li, B. Zhu, J. Sun, H. Gong, J. Yu, L. J. J. o. C. Zhang and I. *Science,* **2024**, 654, 1010-1019.
16. L. Sun, H. Dong, J. Xu, X. Liu and H. Tang, *ACS Sustain. Chem. Eng,* **2023**, 11, 8009-8019.
17. H. Sakurai, M. Kiuchi, T. Jin, *Catal. Commun.***2018**, 114, 124-128.
18. Y. X. Zhang, S. M. Wu, G. Tian, X. F. Zhao, L. Y. Wang, Y. X. Yin, L. Wu, Q. N. Li, Y. X. Zhang, J. S. Wu, C. Janiak, , K. I. Ozoemena, , M.Shalom, X. Y. Yang, *Chem. Eur. J* **2021**, 27, 14202.
19. C. Yang, J. Qin, S. Rajendran, X. Zhang, R. Liu, *ChemSusChem* **2018**, 11, 4077
20. P. Xing, F. Zhou, S. Zhan, *Environ. Res.* **2021**, 197, 111167
21. S. Lv, Y. Wang, Y. Zhou, Q. Liu, C. Song, D. Wang, *Environ. Res.* **2021**, 868, 159144.
22. T. Song, P. Zhang, T. Wang, A. Ali, H. J. N. Zeng, Nanoscale **2018**, 10, 2275-2284.
23. S.-T. Xiao, R. Yin, L. Wu, S.-M. Wu, G. Tian, M. Shalom, L.-Y. Wang, Y.-T. Wang, F.-F. Pu, H.-N. Barad, *Nano Lett.* **2023**, 23, 4390-4398.
24. S. Liu, Y. Ma, D. Chi, Y. Sun, Q. Chen, J. Zhang, Z. He, L. He, K. Zhang, B. Liu, *Int. J. Hydrog. Energy* **2022**, 47, 9220.
25. C. Zhu, C. a. Liu, Y. Fu, J. Gao, H. Huang, Y. Liu, Z. Kang, *Appl. Catal. B: Environ* **2019**, 242, 178.
26. A.-J. Simamora, T.-L. Hsiung, F.-C. Chang, T.-C. Yang, C.-Y. Liao, H. P. Wang, *Int. J. Hydrog. Energy* **2012**, 37, 13855.
27. Y. Tang, Y. Sun, Y. Li, Y. Guo, B. Liu, X. Tan, Z. Hu, D. Zhong, J. Ye, T. Yu, *Adv. Funct. Mater.* **2024**, 2405527